

Optimization of the BiO₈ polar group of BiVO₄ by Cl⁻-embedded modification to manipulate bulk-surface carrier separation for achieving efficient Piezo-PEC water oxidation

Lihao Liu^a, Mengnan Ruan^{a,b}, Chengyi Wang^{a,b}, Zhifeng Liu^{a,b,*}

^a School of Materials Science and Engineering, Tianjin Chengjian University, Tianjin 300384, China

^b Tianjin Key Laboratory of Building Green Functional Materials, Tianjin Chengjian University, Tianjin 300384, China

ARTICLE INFO

Keywords:

BiVO₄
Cl⁻-embedded modification
Polar group
Piezoelectric polarized electric field
PEC water oxidation

ABSTRACT

BiVO₄ is a promising photoanode material. However, achieving only a 2.67 % maximum ABPE while having a theoretical solar conversion efficiency of 9.2 % highlights the need for an effective carrier regulation strategy. In this study on the piezoelectric material BiVO₄, Cl⁻-embedded modification through synthetic post-treatment changes the oxygen evolution reaction (OER) pathway and suppresses surface charge recombination. In addition, the surprising finding of Cl⁻ bonding with Bi³⁺ causing distortion in the BiO₈ polar groups not only enhances the piezoelectric response but also significantly improves the performance of piezo-photoelectric chemical (Piezo-PEC) water oxidation. In the absence of any co-catalyst or sacrificial agent, the photocurrent density of Cl⁻-embedded modified BiVO₄ reached 0.268 mA/cm² at 1.23 V_{RHE} (5 times that of bare BiVO₄). The data indicate that the piezoelectric polarized electric field successfully reduces electron-hole recombination. Cl⁻-embedded modification amplifies the electric field intensity of the surface electric dipole in an ultrasonic environment, facilitating hole access to the catalytically active sites on the surface. Furthermore, the modified surface layer creates a rapid channel for hole migration, with the hole trapping process intricately linked to isolated electrons and intermediate Cl atoms. This embedded modification of polar groups serves as a reference for further exploration into the macroscopic polarization of piezoelectric materials and offers an optimization concept for the field of Piezo-PEC catalysis.

1. Introduction

Humanity is confronted with the escalating challenges of energy scarcity and environmental degradation, necessitating the expedient adoption of economically sustainable fuel sources. The photo-electrochemical "artificial green leaf" technology, emulating the photosynthetic processes of plants, harnesses solar energy to catalyze water decomposition, yielding clean fuel in the form of high-calorific-value green hydrogen. Characterized by minimal energy consumption and zero pollution, this approach has garnered significant interest within the realm of renewable energy conversion [1,2]. The semiconductor light absorber, as the "green leaf" in artificial photosynthesis, plays a pivotal role in absorbing sunlight, facilitating the separation and transfer of photogenerated carriers, and catalyzing surface redox reactions. Among its fundamental properties, the band structure of the semiconductor stands out as paramount, directly influencing the efficacy of PEC water

oxidation. The band gap (E_g) needs to be sufficiently small for broad sunlight absorption, while the band positions should facilitate water oxidation and reduction, thus lowering the photocurrent onset potential [3,4].

BiVO₄ possesses an optimal bandgap of 2.4 eV, with conduction band (CB) and valence band (VB) positions conducive to electron conduction. In contrast to traditional semiconductor TiO₂, BiVO₄ exhibits superior visible light absorption capabilities, rendering it more apt for water electrolysis applications. Regrettably, BiVO₄ encounters challenges in practical applications due to its low electron mobility, leading to the recombination of photogenerated carriers. Additionally, water oxidation presents a thermodynamically unfavorable process, necessitating the transfer of four electrons to yield a single O₂ molecule, thus rendering the process kinetically sluggish [5,6]. Over the past decades, researchers have made significant strides in addressing these issues through techniques such as constructing heterojunctions [7],

* Corresponding author at: School of Materials Science and Engineering, Tianjin Chengjian University, Tianjin 300384, China.

E-mail address: tjulzf@163.com (Z. Liu).

<https://doi.org/10.1016/j.apcatb.2024.124117>

Received 5 April 2024; Received in revised form 18 April 2024; Accepted 23 April 2024

Available online 24 April 2024

0926-3373/© 2024 Elsevier B.V. All rights reserved.

incorporating cocatalysts [8], and employing external ion doping [9]. However, the persistent issue of high electron-hole recombination efficiency remains a formidable obstacle, demanding the exploration of further strategies to overcome this bottleneck.

It is noteworthy that halogen modification/doping has emerged as a promising strategy to address the aforementioned challenges. For instance, Zhang et al.'s research [10] utilizes fluorine (F) modification to orient the dipole moment of interfacial water molecules towards the WO_3 surface. Consequently, interfacial water molecules experience increased difficulty in initiating the initial step of the water oxidation reaction, thereby facilitating the desorption of HO^* and O-O^* , thereby promoting the 2-electron water oxidation reaction. Remarkably, recent studies have begun to challenge the conventional notion that chlorine (Cl) acts as a catalyst poisoning element [11,12]. In the mid-20th century, biologists observed chlorine's significant impact on oxygen release rates. Furthermore, early findings indicated that halogens could impede carrier recombination via polarization effects. Surface modification with an anion possessing suitable electronegativity, like Cl^- , can induce anion polarization, aiding in the capture of photo-generated holes and thereby prolonging carrier lifetime [13].

Simultaneously, the emerging field of piezoelectric-photoelectric chemistry (Piezo-PEC), derived from PEC, has garnered increasing attention [14,15]. The basic principle of the piezoelectric effect is to utilize external mechanical energy (e.g., wind or tidal energy) into periodic stress applied to the photoelectrode. This stress induces the separation of positive and negative charge centroids within the cell, thereby generating an internal electric field and facilitating the separation and transport of photogenerated charge carriers. Currently, numerous piezoelectric materials have been explored for piezoelectric-photoelectric catalysis, including NaNbO_3 [16,17], BaTiO_3 [18,19], Bi_2MoO_6 [20,21], BiFeO_3 [22,23], and others. For instance, Singh et al. [24] demonstrated that ultrasonic vibration-induced alternating internal potentials within NaNbO_3 nanostructures significantly enhance the efficiency of charge separation for photogenerated carriers. Leveraging piezoelectricity, the photocurrent density of NaNbO_3 increased from 0.78 mA/cm^2 to 1.02 mA/cm^2 . These investigations underscore the potential of Piezo-PEC as an emerging technology poised to enhance the performance of photoelectric catalytic materials by exploiting the piezoelectric effect, thereby advancing renewable energy conversion and related domains.

Among various piezoelectric materials, monoclinic scheelite BiVO_4 (s-m) stands out for its exceptional piezoelectric properties attributed to its unique chemically bonded layer stacks [25]. This layered configuration facilitates efficient carrier transport, while the presence of BiO_8 and VO_4 polar groups enables piezoelectric catalysis in BiVO_4 [26,27]. Research has demonstrated that the internal polar field, stemming from the spontaneous polarization of BiVO_4 , catalyzes the hydrogen evolution reaction, with the internal polar field effect enhancing carrier separation [28]. However, research on modifying polar groups in BiVO_4 , particularly their application in Piezo-PEC water decomposition, remains limited. Naturally, it is interesting to associate polar groups with anionic polarization. Undoubtedly, this holds substantial scientific and engineering importance in photoelectrochemical energy conversion.

Here, we demonstrate a photoanode with high Piezo-PEC water oxidation performance based on Cl^- modified BiVO_4 films, and deeply study the influence mechanism of Cl^- -embedded modification polar groups and internal electric field on BiVO_4 . This study represents the first elucidation of enhanced bulk-surface charge separation efficiency through the perspective of embedded polar groups, offering a viable approach for tailoring non-intrinsic surface states of piezoelectric materials to achieve efficient Piezo-PEC water oxidation.

2. Experimental section

2.1. Preparation of sample

In accordance with prior research [29], BiVO_4 films were fabricated on a conductive substrate of fluorine-doped tin oxide (FTO, resistance 7Ω , dimensions $1.5 \text{ cm} \times 3.0 \text{ cm}$). The synthesis involved using bismuth ($\text{Bi}(\text{NO}_3)_3 \cdot 5\text{H}_2\text{O}$) pentahydrate as the bismuth source and Ammonium vanadate (NH_4VO_3) as the vanadium source through a solvothermal combined with ion exchange approach. Considering that NH_4^+ did not affect the crystal structure of BiVO_4 during the ion exchange process, NH_4Cl solution was used in the impregnation method to prevent positive impurity ions from affecting the experimental results. To facilitate comparison, the BiVO_4 samples were immersed in NH_4Cl solutions of varying concentrations (0.3 M, 0.5 M, 0.7 M) for a duration of 12 h. Subsequently, the resulting products were collected, rinsed with a small amount of deionized water, and dried in a 70°C oven for 10 h. The resulting samples were denoted as $\text{Cl}(\text{L}):\text{BiVO}_4$, $\text{Cl}(\text{M}):\text{BiVO}_4$, and $\text{Cl}(\text{H}):\text{BiVO}_4$, respectively. The specific procedure for these operations is depicted in Fig. 1. Raw materials and details of the BiVO_4 film preparation process are given in the Supplementary information.

2.2. Characterization

X-ray diffraction (XRD) analysis, conducted on a Rigaku-D/max-2500 instrument with $\text{Cu K}\alpha$ radiation at 40 kV and 150 mA, was employed to confirm the crystal structure of the sample over a 2θ range of $15\text{--}70^\circ$. Scanning electron microscopy (SEM) utilizing a JEOL JSM-7800F instrument, coupled with energy-dispersive spectroscopy (EDS) and X-ray photoelectron spectroscopy (XPS) using a Thermo ESCALAB 250XI with $\text{Al-K}\alpha$ X-ray, provided insights into the microscopic morphological characteristics, elemental composition, and distribution of the samples. transmission electron microscopy (TEM) on a Tecnai G2 Model 20 and high-resolution transmission electron microscopy (HRTEM) were utilized to examine the morphological and lattice details of the samples. Fourier-transform infrared spectroscopy (FTIR) analysis was conducted at room temperature using a Nicolet 380 spectrophotometer with a spectral range of $500\text{--}4000 \text{ cm}^{-1}$ and a resolution of 4 cm^{-1} . Furthermore, the spectral response range of the samples was recorded via a DU-8B UV-Vis spectrophotometer, enabling the calculation of the optical band gap energy:

$$E_g = 1240/\lambda_{\text{Absorp Edge}} \quad (1)$$

$$(\alpha h\nu)^n = A(h\nu - E_g) \quad (2)$$

the equation provided represents the relationship between the absorption coefficient (α), incident frequency (ν), Planck's constant (h), band gap (E_g), and a constant (A). In the case of BiVO_4 , which is a direct

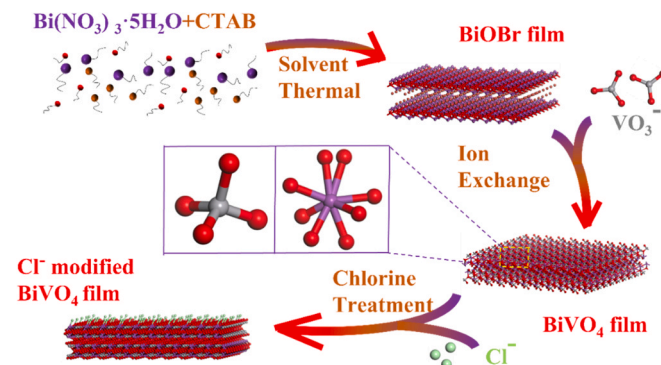


Fig. 1. The fabrication process of Cl^- modified BiVO_4 nanosheets includes self-assembly, ion exchange and impregnation treatment processes.

semiconductor, n equals 2 [30]. Photoluminescence (PL) emission spectra were acquired using a FLS980 series fluorescence spectrometer. Additionally, to explore the kinetic details of surface charge separation, surface photovoltage (SPV) measurements were conducted. This involved utilizing a device comprising a monochromatic light source (500 W Xe lamp), a lock-in amplifier (SR830), a sample chamber, and a surface photovoltage spectrometer (PL-SPS/IPCE1000). The photoelectric chemical test system was combined with Labsolar 6A all-glass automatic on-line trace gas analysis system to obtain Faraday efficiency. The enhanced contact angle meter of the R1R100H-0-60 equipment was used to characterize the hydrophilicity of all samples. Moreover, PFM measurements were carried out at the modulation frequency with the aid of a lock-in amplifier (Bruker Multimode 8).

2.3. PEC and Piezo-PEC measurements

The PEC (Photoelectrochemical) properties of the samples were assessed using a constant potential electrochemical workstation, specifically the CHI760E model from Changhua, Shanghai, China. The experimental setup included an Ag/AgCl reference electrode and a platinum (Pt) sheet serving as the counter electrode. To simulate solar illumination, a 300 W xenon lamp was employed, with a 1.5 G filter to regulate the light intensity to 100 mW cm^{-2} . The electrolyte utilized in the experiments was a 0.5 M Na_2SO_4 solution. The measured potential values were converted into the scale of reversible hydrogen electrode (RHE) using the Nernst equation [31]:

$$E(\text{vs RHE}) = E(\text{vs Ag/AgCl}) + 0.0591 \times \text{pH} + 0.1976 \quad (3)$$

The current density-voltage (J-V) curves were acquired using linear scanning voltammetry (LSV) over the voltage range from 0 V to $1.23 \text{ V}_{\text{RHE}}$ at a scan rate of 10 mV s^{-1} . The sample's electrochemical impedance spectrum (EIS) was measured across frequencies ranging from 1 to 105 Hz with a sinusoidal AC amplitude of 10 mV. Impedance test analysis yielded Mott-Schottky (M-S) data from 1 to 1000 Hz, providing the applied density (N_d) and flat-band potential (V_{FB}) according to the following equation [32]:

$$1/C^2 = (2/e_0\epsilon\epsilon_0A^2N_d)[V - V_{\text{FB}} - (K_B T/e_0)] \quad (4)$$

$$N_d = (2/e_0\epsilon\epsilon_0)[d(1/C^2)/dV]^{-1} \quad (5)$$

in the given equation, C represents the space charge capacitance, while ϵ and ϵ_0 denote the vacuum and relative dielectric constants of BiVO_4 , respectively. e_0 signifies the fundamental charge, A stands for the coated area of the working electrode (1 cm^2), and V represents the applied bias voltage. Additionally, K_B is the Boltzmann constant ($1.38 \times 10^{-23} \text{ J K}^{-1}$), and T denotes the temperature in Kelvin.

The applied bias photon-to-current efficiency (ABPE) for water splitting was calculated using the following equation [33]:

$$\text{ABPE}(\%) = [(J_p \times (1.23 - V_{\text{bias}}))/(P_{\text{in}})] \times 100\% \quad (6)$$

where J_p is the photocurrent density from the workstation, V_{bias} is the applied voltage, and P_{in} is the power of the solar simulator (100 mW/cm^2).

The charge separation efficiency (η_{bulk}) and charge injection efficiency (η_{surface}) were determined by the following equation [34] to investigate the factors contributing to the increased optical current density.

$$\eta_{\text{bulk}}(\%) = (J_{\text{Na}_2\text{SO}_3}/J_{\text{abs}}) \times 100\% \quad (7)$$

$$\eta_{\text{surface}}(\%) = (J_{\text{H}_2\text{O}}/J_{\text{Na}_2\text{SO}_3}) \times 100\% \quad (8)$$

$J_{\text{H}_2\text{O}}$ represents the photocurrent density, while J_{abs} denotes the current density corresponding to photon absorption. Additionally, $J_{\text{Na}_2\text{SO}_3}$ indicates the photocurrent density measured in an electrolyte

containing 0.25 M Na_2SO_3 as a hole scavenger, added to 0.5 M Na_2SO_4 .

The piezoelectric coefficient (d_{33}) is calculated from Eq. (9) [35]. This coefficient quantifies the response of external mechanical forces acting on the object.

$$d_{33} = \text{LS PR amplitude} \times \text{deflection sen}/16/\text{LS PR AC bias} \quad (9)$$

the term "amplitude" refers to the maximum peak value of the butterfly-shaped curve. "Deflection sen" is derived from the pressure-generated curve. Q = peak height/half peak width/ $\sqrt{2}$. "AC" denotes the alternating current utilized during the testing process. "LS" signifies load sensing, while "PR" represents piezoresistive.

FE (Coulomb Efficiency), measures charge transfer efficiency in electrochemical reactions. It indicates the percentage of charge utilized by the actual product compared to the theoretical product, essential for evaluating electrode performance. The calculation formula is as follows:

$$\text{FE}(\text{O}_2) = \alpha nF/Q = 4nF/(I \times t) \times 100\% \quad (10)$$

In the equation $\alpha = 4$ (for product O_2), n represents the actual amount of product (mol), F is the Faraday constant ($96,485.34 \text{ C/mol}$), Q denotes the theoretical charge used (C), I represent the photocurrent generated (A), and t stands for the reaction time (s).

Additionally, the Piezo-PEC test activates the piezoelectric effect of the samples by applying ultrasound during the PEC test described above.

3. Results and discussion

The crystal structures of both the original BiVO_4 and the $\text{Cl}(\text{X}):\text{BiVO}_4$ ($\text{X} = \text{L}, \text{M}, \text{H}$) films deposited on the FTO conductive substrate were characterized using XRD analysis, as illustrated in Fig. S1. At angles of 18.7° , 28.9° , and 47.3° , three prominent peaks (1 1 0), (1 2 1), and (0 4 2) denoted by "◆" are attributed to the monoclinic scheelite structure of BiVO_4 , with no additional diffraction peaks observed, indicating the preservation of BiVO_4 's crystal structure following Cl^- modification. All samples exhibit a diffraction pattern consistent with the single phase of BiVO_4 , referencing the JCPDS database file 14-0688. Additionally, the diffraction peak attributed to the FTO conductive substrate, labeled "♥", is indexed as SnO_2 (JPCDS no. 77-0452), serving as an inherent signal. Ionic polarization is well-established to induce alterations in the crystal lattice. A closer examination within the range of $28\text{--}30^\circ$ reveals a shift in the diffraction peak of the (1 2 1) crystal face, attributed to anion polarization stemming from Cl^- surface modification. SEM images depicted in Fig. 2(a, b), and Fig. S2 (a, b) illustrate the morphological changes of BiVO_4 pre- and post- Cl^- modification. The top view showcase the retention of BiVO_4 's characteristic nanosheet structure, uniformly and vertically interposed on the FTO glass substrate. Furthermore, it can be seen from Fig. 2(b) that the surface of BiVO_4 has become rough due to Cl^- modification, which may be related to the improvement of Piezo-PEC performance. The HRTEM images (Fig. 2(e)) reveal a lattice surface spacing of 0.31 nm, corresponding to the (1 2 1) crystal face of monoclinic scheelite BiVO_4 . The TEM-EDS mapping in Fig. 2(g) confirms the successful embedding of Cl^- on the surface of BiVO_4 . Furthermore, Fig. 2(d) demonstrates the formation of an approximately 5 nm thick amorphous layer on the surface of BiVO_4 samples treated with ammonium chloride, indicating the highly efficient etching capability of Cl^- . The consistent crystal phase suggests that the introduction of Cl^- does not induce lattice distortion or introduce new nanolayers, a notion supported by FTIR analysis (Fig. S3 (c)). The band around 780 cm^{-1} , stemming from the antisymmetric contraction vibration of bound oxygen (V-O-V) shared by two vanadium atoms, exhibits nearly unchanged intensity pre- and post- Cl^- modification, indicating the unchanged coordination environment of V^{5+} . The band at 615 cm^{-1} corresponds to the symmetric contraction pattern of the V-O-V angle. Furthermore, the variation around 1591 cm^{-1} may be attributed to the BiO_8 group, accompanied by a significant dipole moment change during vibration. Additionally, two prominent bands at 1662 and 3449 cm^{-1} are

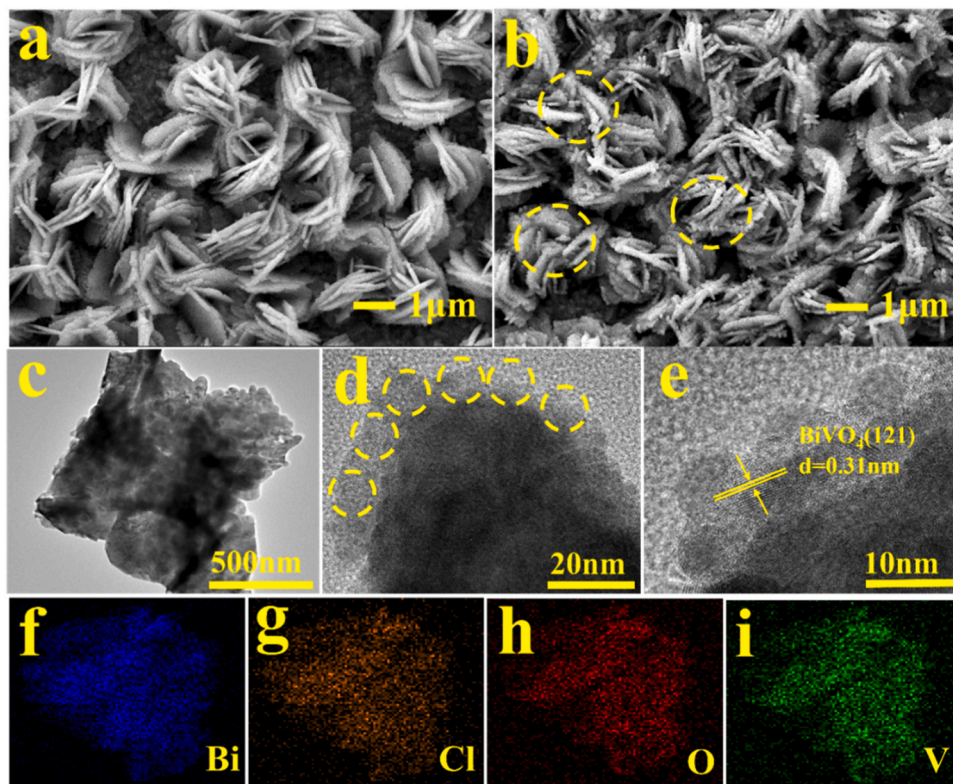


Fig. 2. SEM images of (a) pristine BiVO_4 and (b) Cl(M):BiVO_4 ; (c) The TEM (d, e) HRTEM images and (f–i)TEM-EDS mapping of Cl(M):BiVO_4 .

associated with the O–H stretching and bending vibrations of water molecules adsorbed on the particle surface [36]. The EDS diagram (Fig. 2(d)) illustrates the uniform distribution of Bi, V, O, and Cl elements within Cl(M):BiVO_4 . To delve deeper into the chemical states of surface elements post Cl^- modification, a comprehensive spectrum is presented in Fig. S3 (a). The presence of Cl is corroborated by Cl 2p peaks centered at 199.7 eV and 197.9 eV. The Bi 4f peaks of the BiVO_4 film at 163.5 eV and 158.2 eV are attributed to Bi^{3+} (Fig. 3(a)). Notably, the Bi^{3+} peaks of Cl(M):BiVO_4 shifted by 0.4 eV to 163.9 eV and 158.6 eV, respectively, due to the strong electronegativity of Cl[−] changing the chemical environment. The shift of the Bi^{3+} peak can reasonably be assumed that Cl^- is bonded to the Bi^{3+} position [37]. Additionally, XPS analysis reveals a surface Cl concentration of 2.7 wt%

in the optimized sample, further confirming successful sample preparation.

The catalyst's optical properties and bandgap values were assessed via UV–Vis diffuse reflectance spectroscopy (Fig. S3 (b)). Both original BiVO_4 and Cl(M):BiVO_4 samples were examined. The UV–Vis spectral curve of BiVO_4 exhibits a similar absorption edge at 510 nm, with noticeably increased absorption intensity, suggesting minimal impact of Cl^- modification on the absorption edge but enhanced optical absorption intensity of BiVO_4 . The enhancement of light absorption leads to an increase in the free charge density, which effectively improves the efficiency of water splitting. Additionally, the optical band gap for both original BiVO_4 and Cl(M):BiVO_4 films is determined to be 2.5 eV (inset), consistent with reported values for monoclinic scheelite BiVO_4 in the

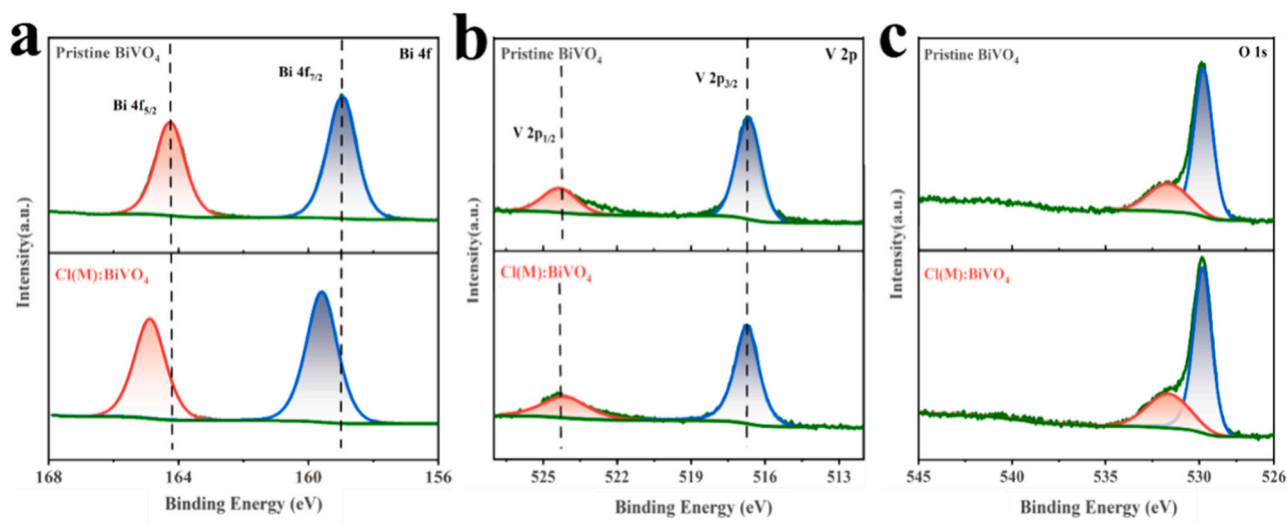


Fig. 3. XPS of pristine BiVO_4 and Cl(M):BiVO_4 : (a) Bi 4f, (b) V 2p, and (c) O 1s.

range of 2.4–2.5 eV (absorption edge: 500–520 nm) [38]. To elucidate the electron-hole separation and transfer process within the BiVO₄ photoelectrode, PL spectroscopy was employed to capture photons emitted by self-trapped excitons. The intensity of the peak reflects the recombination of photogenerated carriers, with higher peaks indicating more significant carrier recombination. Fig. S3 (d) illustrates that BiVO₄ exhibits the highest peak intensity around 510 nm, with Cl(L):BiVO₄, Cl(H):BiVO₄, and Cl(M):BiVO₄ following in descending order. This suggests that Cl⁻ modification may impede the recombination of photogenerated carriers. This effect could stem from Cl⁻ bonding to the Bi³⁺ surface position, creating a hole trapping mechanism. This alteration likely influences the pathway of the oxygen evolution reaction, thereby expediting the separation of photogenerated carriers. It is reasonable to deduce that the hole trapping effect of Cl⁻ correlates with its lone pair electrons and the subsequent formation of intermediate chlorine atoms possessing suitable electronegativity [39]. With increasing NH₄Cl concentration, the intensity of Cl(H):BiVO₄ at a consistent wavelength surpasses that of Cl(M):BiVO₄, suggesting a rising trend in photogenerated carrier recombination. Additionally, to delve deeper into surface potential shifts induced by excitation charges under various light wavelengths, we conducted SPV spectra tests on all samples (Fig. S4). Under light excitation, all samples exhibit a positive charge generation on the surface, characteristic of N-type semiconductors. Furthermore, the surface photovoltaic response at the same wavelength initially rises and then declines with increasing Cl⁻ modification levels. This indicates that appropriate Cl⁻ modification on the BiVO₄ surface can effectively hinder the recombination of surface photogenerated charges. The experimental findings demonstrate that Cl⁻ modification of the BiVO₄ film represents an efficient strategy to enhance PEC performance by optimizing the reaction pathway, thereby facilitating the migration of more holes to the surface, and expediting the oxygen evolution reaction.

To investigate the sample's piezoelectric properties, we employed the PFM technique. We examined the local point-to-point piezoelectric responses of both Pristine BiVO₄ and Cl(M):BiVO₄ nanostructured films on FTO substrates, applying a ± 10 V probe bias. This local piezoelectric signal effectively illustrates the piezoelectric effect induced by ultrasonic stress. Fig. 4(a, b) shows the 3D topography of the surface of Pristine BiVO₄ and Cl(M):BiVO₄ films in PFM experiments, respectively. Additionally, Fig. 4(c, f) illustrate the microscopic morphology of the surface for Pristine BiVO₄ and Cl(M):BiVO₄, respectively, showcasing nanometer sheet material consistent with SEM characterization. Fig. 4(d, e, g, h) depict the piezoelectric response phase and amplitude images of Pristine BiVO₄ and Cl(M):BiVO₄ films obtained via the probe, revealing their piezoelectric characteristics. The piezoelectric amplitude and phase changes of Cl(M):BiVO₄ are more pronounced than those of Pristine BiVO₄ under identical conditions. Fig. 5(a, c) and Fig. 5(d, f)

represent the amplitude and phase signals of PFM, respectively. The amplitude signal signifies the polarization's magnitude, whereas the phase signal denotes its orientation. Pristine BiVO₄ films displayed noticeable phase hysteresis and amplitude butterfly loops, indicating their ferroelectric characteristics. However, the film's minimal phase hysteresis, as evidenced by a small loop area, suggests weak ferroelectric properties likely attributed to BiVO₄'s semiconductor nature. Surprisingly, the phase hysteresis and polarization amplitude of Cl(M):BiVO₄ are obviously improved compared with pristine BiVO₄, which indicates that Cl⁻ modification has a positive effect on the piezoelectric response of BiVO₄. In addition, we determined the piezoelectric coefficient (*d*33) from the PFM amplitude data (Fig. 5(b, e)) to quantify the net polarization of the sample. Pristine BiVO₄ exhibits a *d*33 value of 11.67 pm/V, while Cl(M):BiVO₄ demonstrates a significantly higher value of 74.13 pm/V. The *d*33 value of Cl(M):BiVO₄ is 6.6 times that of Pristine BiVO₄. In accordance with prior studies [40], the catalytic efficacy of monoclinic scheelite BiVO₄ surpasses that of the tetragonal phase primarily due to heightened distortion in the local coordination environment of Bi and V within the monoclinic phase. This distortion fosters local polarization, thereby facilitating the segregation of photogenerated carriers. Moreover, in conjunction with the XPS findings, it becomes evident that Cl⁻ modification induces greater complexity in the coordination environment of Bi within BiVO₄. This modification intensifies the non-central symmetry of BiVO₄'s surface cell, consequently amplifying surface-localized polarization under external forces and expediting the separation of surface photogenerated charges.

The J-V curves of the electrodes were assessed in a 0.5 M Na₂SO₄ electrolyte solution (pH = 6.8) using a three-electrode system. To optimize the photovoltaic performance of the photoanode and to study the effect of the piezoelectric polarization electric field, we maintained the concentration of the NH₄Cl solution at 0.5 M and compared the J-V at different impregnation times (Fig. S5 (a)). Longitudinal comparison revealed that the most favorable properties were achieved with an impregnation time of 12 h. Additionally, to analyze the influence of Cl⁻ and NH₄⁺ in the NH₄Cl solution on enhancing BiVO₄ performance, we examined several reagents including NaCl, NH₄Cl, (NH₄)₂SO₄ and NH₄HCO₃ (Fig. S5 (b)). The findings ruled out the influence of NH₄⁺, thereby underscoring the significant role of Cl⁻ modification in enhancing PEC performance. Moreover, to determine the optimal ultrasonic frequency for inducing the piezoelectric effect, BiVO₄ samples were studied at different frequencies (Fig. S5 (c)). It was evident that BiVO₄ at 90 kHz exhibited the highest current density (1.23 V_{RHE}) under dark conditions. At 90 kHz, BiVO₄ exhibits a 17.9 % higher current density compared to 0 kHz, highlighting the effective promotion of photogenerated carrier separation by the piezoelectric polarized electric field induced by ultrasonic vibration. The experiments further confirm

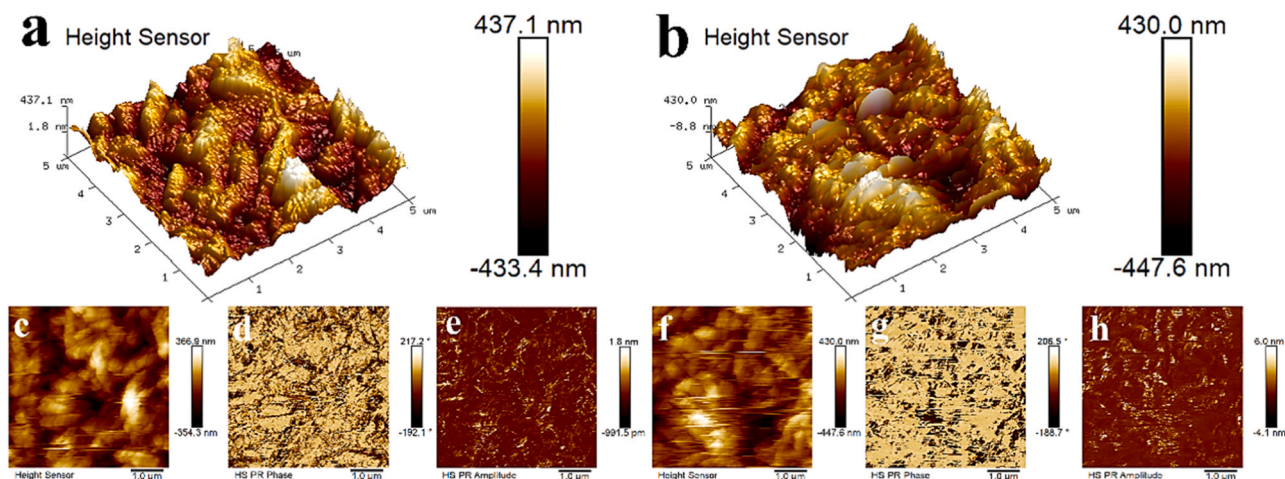


Fig. 4. PFM morphologies, the relative phase and amplitude of the piezoelectric response images of (a, c–e) pristine BiVO₄ and (b, f–h) Cl(M):BiVO₄.

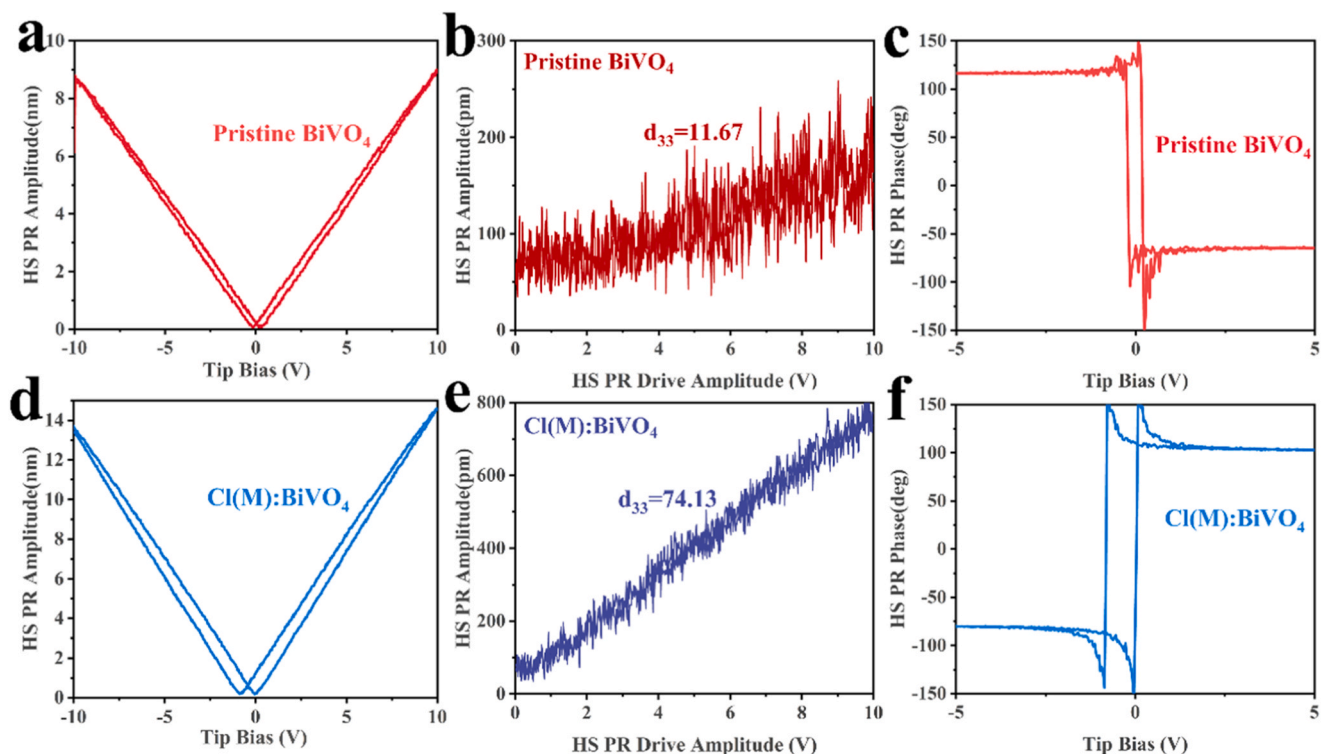


Fig. 5. Amplitude butterfly loop and phase hysteresis loop of (a–c) pristine BiVO_4 and (d–f) Cl(M):BiVO_4 obtained by PFM testing.

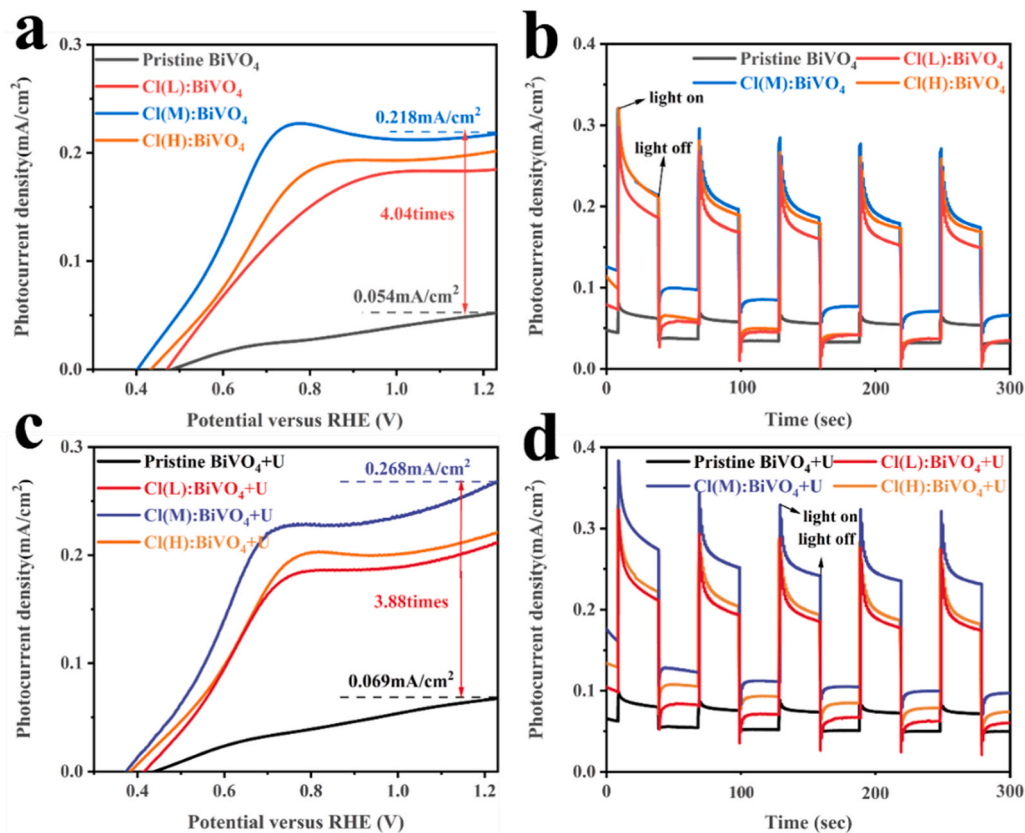


Fig. 6. Under AM1.5 G simulated sunlight, (a) Photocurrent density–voltage (J – V) of photoanodes in 0.5 M Na_2SO_4 ($\text{PH} = 6.52$) and (c) under ultrasound condition; (b) J – t curves of chopped transient photocurrent of photoanodes for 300 s at $1.23 V_{\text{RHE}}$ and (d) under ultrasound condition.

the strong piezoelectric response of BiVO₄ and lend support to the subsequent investigation of the Piezo-PEC properties of the samples at 90 kHz. Samples prepared under optimized conditions were evaluated, as depicted in Fig. 6(a). Notably, Cl(M):BiVO₄ demonstrates a photocurrent density of 0.218 mA/cm² at 1.23 V_{RHE}, approximately four times that of Pristine BiVO₄, which registers 0.054 mA/cm² at 1.23 V_{RHE}. Following appropriate Cl⁻ modification, the initial overpotential of Cl(M):BiVO₄ decreases from 0.48 V for Pristine BiVO₄ to 0.40 V, indicating the capability of Cl(M):BiVO₄ to undergo the hydrogen evolution reaction (HER) at a lower applied voltage. Cl⁻ modification proves effective in inhibiting carrier recombination by altering the surface charge state. At the same time, the piezoelectric characteristic of BiVO₄ is excited by ultrasonic wave. Under the combined action of the stress and the built-in electric field caused by the distribution of piezoelectric potentials on the surface of the material, all samples produce a current response under the ultrasonic field (Fig. 6(c)). Cl(M):BiVO₄ has the largest piezoelectric field current under light conditions (0.268 mA/cm² at 1.23 V_{RHE}), which indicates that the bulk piezoelectric potential driving effect on carriers can be improved by appropriate Cl⁻ modification. It is worth noting that achieving the target potential under the same photocurrent density (0.025 mA/cm², 0.050 mA/cm²) under applied stress, Cl(M):BiVO₄ electrode only needs 0.43 V and 0.48 V overpotential, and the overpotential difference between the front and rear BiVO₄ electrodes is nearly 1.6 times. This shows that the modified catalyst can greatly improve the energy utilization efficiency. Fig. 6(a) compared to Fig. 6(c), the initial overpotential of all samples before and after ultrasound showed a relatively obvious negative shift and the photocurrent density increased significantly, indicating that the driving force provided by the internal electric field generated by the piezoelectric effect could effectively inhibit the recombination of sample phase charges, thus realizing efficient Piezo-PEC water electrolysis.

The J-t diagram of the Cl(M):BiVO₄ photoelectrode was measured under ultrasonic conditions at 6000 s of illumination (Fig. S6 (a)). At the same time, the Faraday efficiency graph (corresponding to O₂) measured under the corresponding photoelectric conditions is given in Fig. S7. The slow decay photocurrent and SEM images before and after the test (Fig. S6 (b, c)) indicate the excellent stability of the sample. The Faraday efficiency improvement of nearly 4 % indicates the superiority of the Cl⁻ modification method. In addition, the OCP curve (Fig. S5 (d)) under short-circuit light irradiation is studied. The J-t diagram of the electrodes under short-circuit light before and after ultrasound (Fig. 6(b)) showed a similar ladder trend, indicating that all samples had excellent photo response performance. For Cl(M):BiVO₄, the photovoltage above that of Pristine BiVO₄, suggesting that Cl⁻ modification on the photoelectrode surface enhances energy band bending at the Cl(M):BiVO₄-solution interface, thereby facilitating the separation of photogenerated carriers. Notably, when the lamp is switched on during the J-t test, transient photocurrent spikes are evident in all Cl⁻ modified samples, attributed to the competition between rapid carrier accumulation and slow surface reactions. Comparatively, Cl(M):BiVO₄ tends to exhibit a flatter peak in contrast to Cl(L):BiVO₄ and Cl(H):BiVO₄, with peak size reflecting accumulated surface charge. Integrating the J-V test results, Cl(M):BiVO₄ emerges as the optimal sample, suggesting that accumulated surface charge on moderately Cl⁻ modified BiVO₄ films can swiftly engage in the oxygen evolution reaction (OER). This observation is further supported by the EIS study (Fig. 8(a)), where the equivalent circuit diagram illustrates the measured data of the modified BiVO₄ sample, revealing a small radius arc whose diameter correlates positively with interface transfer resistance, indicating varying degrees of carrier migration at the BiVO₄ interface due to Cl⁻ modification. Tab. S1 shows that the resistance R_p between the electrode and the electrolyte of Cl(M):BiVO₄ is only 210.4 Ω, which is significantly smaller than other electrodes. The results show that the electron conductivity is significantly improved under moderate Cl⁻ modification, which can effectively promote the separation and transfer of photogenerated charge. After the

introduction of ultrasonic stress (Fig. 6(d)), the relative peak value of Cl(M):BiVO₄ is almost unchanged while the photocurrent density of all samples increases, which corresponds to the smallest R_p under pressurized conditions, indicating that the charge transfer rate accumulated on the surface of the material is accelerated under the action of ultrasonic field, and the piezoelectric polarized electric field effectively improves the photogenerated carrier transport efficiency. In Fig. 8(c), the Cl(M):BiVO₄ and Pristine BiVO₄ curves are composed of the same solution resistance, but the R_p is very different. Cl(M):BiVO₄ is much smaller, indicating that the rapid transfer of hole carriers at the solid-liquid interface promotes the rapid oxidation of water. The results show that more bulk phase charges migrate to the surface under the action of the built-in electric field, and the coupled Cl⁻ surface modification can overcome the severe charge recombination of BiVO₄ and promote the OER reaction together.

From the ABPE curve of the electrode (Fig. 7(a, d)), it is evident that under the action of applied stress, the Cl(M):BiVO₄ photoanode produces a maximum ABPE of 0.117 % at 0.69 V_{RHE}, which surpasses the earlier references [41,42] on BiVO₄-based photoanodes. The ABPE value also exceeds that of Bi₂WO₆ [43] and WO₃ [44] based photoanodes. To better explain the reason for the increase in photocurrent density, the contact angles of all samples are shown in Fig. S8. The hydrophilicity of the film increased with the increase of Cl⁻ on the surface, this is probably caused by Cl⁻ combining with water to form [Cl⁻·(H₂O)_x]. The bulk phase charge separation efficiency (η_{bulk}) and surface charge separation efficiency (η_{surface}) of all samples before and after ultrasound are shown in Fig. 7(b, e) and Fig. 7(c, f) respectively. Under illumination, the η_{bulk} and η_{surface} of Cl(M):BiVO₄ were significantly higher than those of Pristine BiVO₄. This is due to the right amount of surface Cl⁻ enhances the charge separation at the surface, resulting in less charge recombination and better charge injection into the electrolyte. After ultrasonic treatment, the efficiency is further improved, which may be due to the increase of non-central symmetry of BiVO₄ cell under the action of external stress, which improves the piezoelectric polarization intensity of BiVO₄ itself. On the other hand, Cl⁻ modification changes the reaction path of OER and accelerates the surface charge accumulation into the electrolyte. The synergistic effect of the two inhibits the recombination of body phase and surface photogenerated charges, thus achieving the efficient Piezo-PEC performance of BiVO₄. Mott-Schottky (Fig. 8(b, d)) shows that the slope of all samples is positive, indicating that the photoelectrode has been prepared in the N-type semiconductor. The N_d of all samples was calculated by Eq. (5) and summarized with V_{FB} in Tab. S2. In addition, compared with the original BiVO₄ electrode, the slope of Cl(L):BiVO₄ decreased, and then the slope of Cl(H):BiVO₄ showed an upward trend, which meant that moderate NH₄Cl solution concentration was conducive to the improvement of N_d. Mott-Schottky image shows the V_{FB} values of Pristine BiVO₄ and Cl(M):BiVO₄ electrode are 0.25 and -0.21 V, respectively, which are negatively shifted to -0.01 V and -0.29 V under ultrasonic treatment. The negative displacement of V_{FB} indicates that the energy band bending at the interface is greatly increased. This will effectively improve the separation and transfer of photogenerated electron-hole pairs, thereby improving the performance of Piezo-PEC.

Based on the experimental results, it can be reasonably inferred that Cl⁻ modification promotes the separation and hole transfer of photogenerated carriers. The stress induced by ultrasound amplifies the modification effect of Cl⁻, and the internal electric field triggered greatly inhibits the photogenerated electron-hole pair recombination. The synergistic effect of Cl⁻ modification with the piezoelectric effect leads to an increase in the separation efficiency of BiVO₄'s bulk phase and surface charges, resulting in rapid oxidation of water (Fig. 9). To elucidate the underlying principle more clearly, Fig. 10 shows a detailed diagram of the piezoelectric polarization mechanism and possible surface reaction paths. The piezoelectric effect is achieved through the atomic structure and charge distribution in the material, so that during compression or stretching, the atoms move, creating an asymmetry in

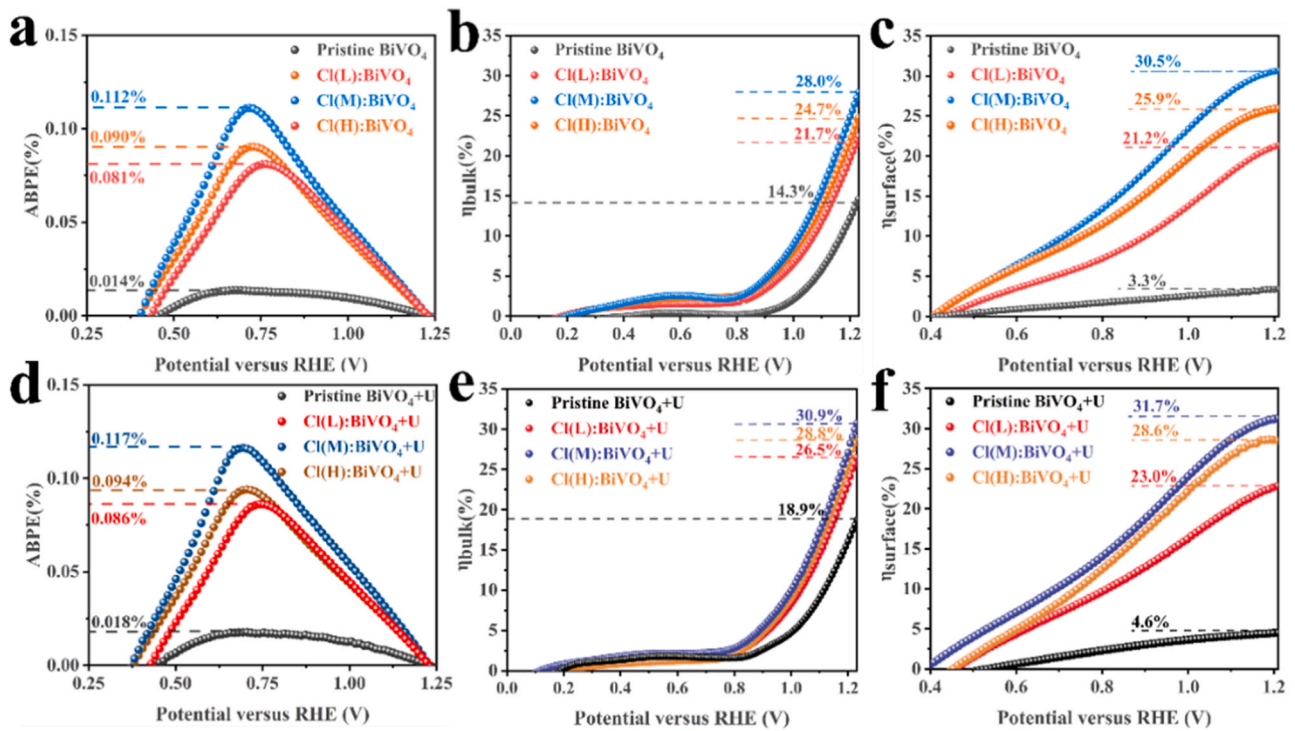


Fig. 7. (a) The applied bias photo-to-current efficiency (ABPE) curves, (b) charge separation efficiency (η_{bulk}), and (c) charge injection efficiency (η_{surface}) of pristine BiVO₄, Cl(X):BiVO₄ (X = L, M, H) photoanodes, along with (d–f) their performance under ultrasound conditions.

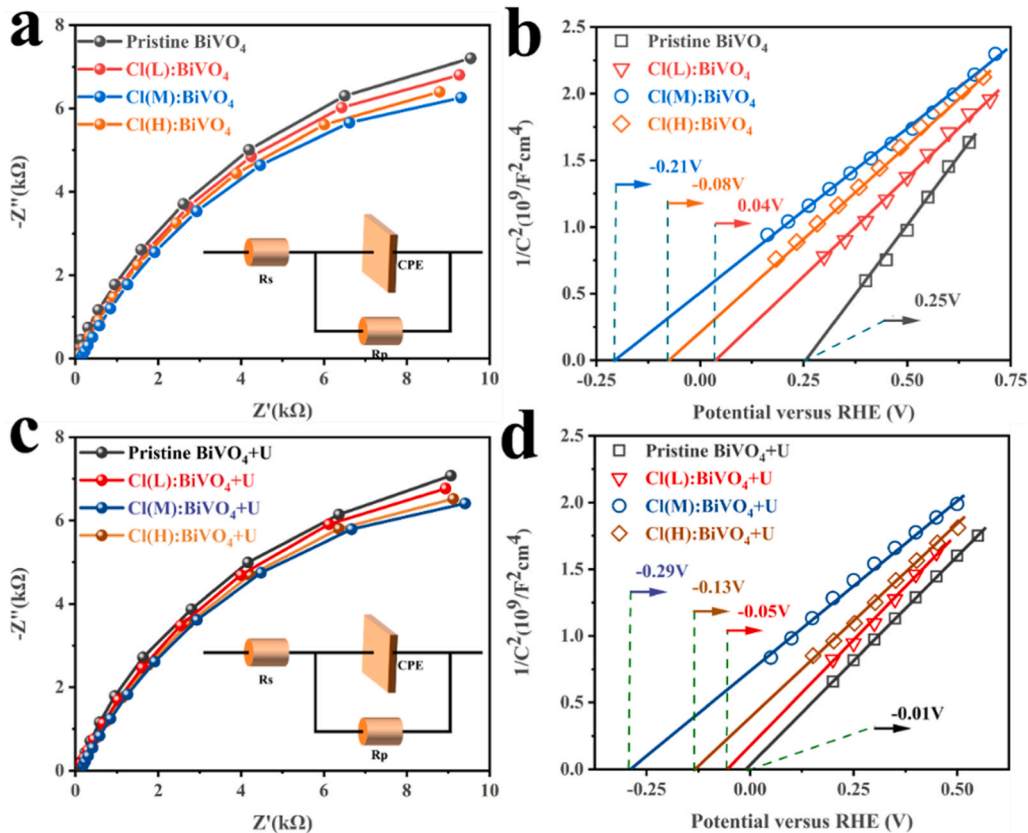


Fig. 8. Under AM1.5 G simulated sunlight, (a) electrochemical impedance spectroscopy (EIS) of photoanodes and (c) under ultrasound condition. In the inset, R_s and R_p denote the solution resistance and polarization resistance in the electrochemical system, respectively, and R_{CPE} denotes the capacitive resistance in the photoanode; (b) Mott-Schottky plots of photoanodes and (d) under ultrasound condition.

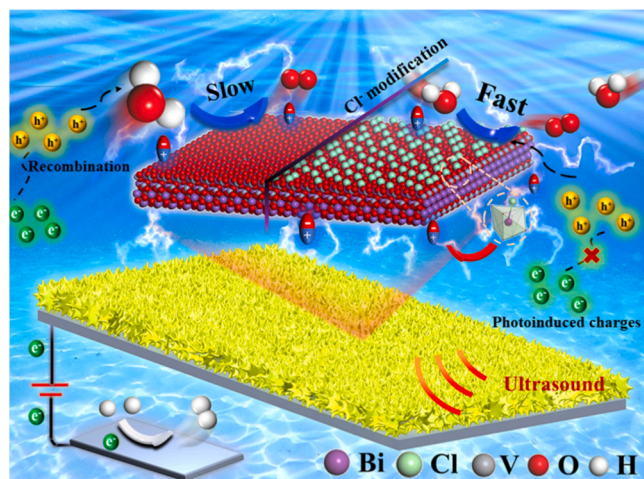


Fig. 9. The mechanism diagram of pristine BiVO₄ and Cl(M):BiVO₄ photoanode under ultrasound condition applied in Piezo-PEC water splitting.

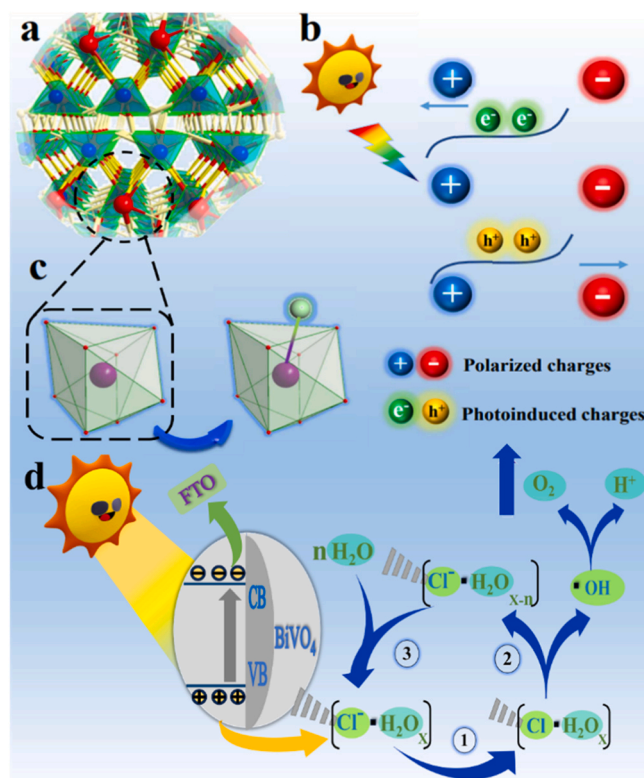


Fig. 10. (a) The crystal structure of BiVO₄; (b) The scheme of polarization promoted bulk charge separation; (c) The schema of Cl⁻ modified BiO₈ dodecahedron; (d) Schematic illustration of photogenerated holes transfer and its reaction with water molecule to evolve O₂ on the Cl⁻ modified BiVO₄.

the dipole. From the crystal structure diagram of BiVO₄ (Fig. 10 (a)) and the local magnification diagram (Fig. 10 (c)), it can be observed that the bismuth vanadate cell is composed of pyramidal structure VO₄ tetrahedron and twisted BiO₈ dodecahedron. The BiO₈ dodecahedron Bi has a positive charge and O has a negative charge, and when bismuth vanadate is squeezed, the dipoles no longer cancel each other out, resulting in a net negative charge and a net positive charge. Under Cl⁻ modification, the non-centrosymmetric amplification of polar groups on the surface increases the net charge. The net charge distribution generated in the volume phase is repeated by countless cells to form a voltage with the

surface, thus effectively separating the photogenerated charge (Fig. 10 (b)). At the same time, excess Cl⁻ will prevent the adsorption of H₂O on the BiVO₄ surface, because Cl⁻ and Bi³⁺ are coordinated on the BiVO₄ surface. This explains why Cl(M):BiVO₄ has the strongest performance in splitting water, but further increasing the concentration of Cl⁻ leads to a decline in performance. Thus, the enhancement of surface polar group to performance has a maximum threshold, indicating that an increase in their number does not necessarily lead to better outcomes. There exists a delicate balance between the promotion effect of Cl⁻ modification and water molecule adsorption. Finally, the Cl⁻ modified OER reaction can be roughly divided into three steps (Fig. 10 (d)). Initially, modified BiVO₄ captures photogenerated holes, generating Cl atoms [−Cl·(H₂O)_x] as stable radicals. Subsequently, these Cl atoms oxidize complex water molecules to generate ·OH, leading to O₂ evolution, while transitioning to the anionic state [−Cl⁻·(H₂O)_{x-n}]. Finally, the anionic state reverts to its original form, [−Cl⁻·(H₂O)_x], through coordination with water molecules.

4. Conclusion

In summary, our study focused on harnessing the unique piezoelectric effect facilitated by the distinctive VO₄, BiO₈ polar group unit within the crystal structure of BiVO₄. Notably, we pioneered the modification of BiVO₄'s polar group using Cl⁻ to improve the performance of Piezo-PEC. XPS, FTIR, and TEM results reveal that Cl⁻ is bonded to Bi³⁺, predominantly concentrated on the surface of the modified BiVO₄. In the ultrasonic environment, the resulting Cl(M):BiVO₄ photoanode exhibited a significantly elevated photocurrent density of 0.268 mA/cm² at 1.23 V_{RHE}, surpassing Pristine BiVO₄ by fivefold. Moreover, its d33 value measured at 74.13 pm/V stands approximately 6.6 times higher than that of the Pristine BiVO₄ photoanode. The excellent Piezo-PEC performance can be attributed to the promoting effect caused by the built-in electric field and surface modification by Cl⁻. The built-in electric field efficiently suppresses bulk charge recombination, while moderate surface modification can effectively adjust the polarity groups (BiO₈) and optimize the oxygen evolution reaction (OER) steps, allowing more charge carriers migrating along the surface to participate in the catalytic process. In this study, the role of photoanode Cl⁻-embedded modification in surface OER reaction was elucidated, and the reason for the improvement of Piezo-PEC performance was explained from the perspective of polar groups for the first time. This simple embedded modification method not only ensures the possibility of large-scale production of the optimized BiVO₄, but also provides a new way to improve the performance of other photoelectrodes.

CRediT authorship contribution statement

Lihao Liu: Writing – original draft, Methodology, Investigation, Data curation. **Mengnan Ruan:** Writing – original draft, Methodology, Investigation, Formal analysis. **Chengyi Wang:** Writing – review & editing, Investigation. **Zhifeng Liu:** Writing – review & editing, Investigation, Funding acquisition.

Declaration of Competing Interest

There are no conflicts of interest.

Data availability

Data will be made available on request.

Acknowledgements

The authors gratefully acknowledge financial support from National Natural Science Foundation of China (Nos. 52373301 and 52073200) and Natural Science Foundation of Tianjin (No. 23JCZDJC00180).

Appendix A. Supporting information

Supplementary data associated with this article can be found in the online version at [doi:10.1016/j.apcatb.2024.124117](https://doi.org/10.1016/j.apcatb.2024.124117).

References

- [1] N. Srinivasan, M. Anbuezhayan, S. Harish, S. Ponnusamy, Efficient catalytic activity of BiVO₄ nanostructures by crystal facet regulation for environmental remediation, *Chemosphere* 289 (2022) 133097–133111.
- [2] K. Chen, R. Wang, Q. Mei, F. Ding, H. Liu, G. Yang, B. Bai, Q. Wang, Spinel-covered interlayer MgO enhances the performance of BiVO₄ photocatalytic ammonia synthesis, *Appl. Catal. B: Environ. Energy* 344 (2024) 123670.
- [3] P. Wang, S. Fan, X. Li, J. Duan, D. Zhang, Modulating the molecular structure of graphitic carbon nitride for identifying the impact of the piezoelectric effect on photocatalytic H₂O₂ production, *ACS Catal.* 13 (2023) 9515–9523.
- [4] Z. Wang, Y. Guo, M. Liu, X. Liu, H. Zhang, W. Jiang, P. Wang, Z. Zheng, Y. Liu, H. Cheng, Y. Dai, Z. Wang, B. Huang, Boosting H₂ production from a BiVO₄ photoelectrochemical biomass fuel cell by the construction of a bridge for charge and energy transfer, *Adv. Mater.* 34 (2022) 1594–1604.
- [5] S. Tu, Y. Guo, Y. Zhang, C. Hu, T. Zhang, T. Ma, H. Huang, Piezocatalysis and piezo-photocatalysis: catalysts classification and modification strategy, reaction mechanism, and practical application, *Adv. Funct. Mater.* 30 (2020) 5158–5189.
- [6] M. Wang, B. Wang, F. Huang, Z. Lin, Enabling piezopotential in piezoelectric semiconductors for enhanced catalytic activities, *Angew. Chem. Int. Ed.* 58 (2019) 7526–7536.
- [7] Q. Yang, G. Tan, L. Yin, W. Liu, B. Zhang, S. Feng, Y. Bi, Y. Liu, T. Liu, Z. Wang, H. Ren, A. Xia, Full-spectrum broad-spectrum degradation of antibiotics by BiVO₄@BiOCl crystal plane S-type and Z-type heterojunctions, *Chem. Eng. J.* 467 (2023) 143450–143463.
- [8] J. Zhang, X. Wei, J. Zhao, Y. Zhang, L. Wang, J. Huang, H. She, Q. Wang, Electronegative Cl[−] modified BiVO₄ photoanode synergized with nickel hydroxide cocatalyst for high-performance photoelectrochemical water splitting, *Chem. Eng. J.* 454 (2023) 140081–140090.
- [9] D. Philo, S. Luo, C. He, Q. Wang, F. Ichihara, L. Jia, M. Oshikiri, H. Pang, Y. Wang, S. Li, G. Yang, X. Ren, H. Lin, J. Ye, Lattice distortion engineering over ultrathin monoclinic BiVO₄ nanoflakes triggering AQE up to 69.4 % in visible-light-driven water oxidation, *Adv. Funct. Mater.* 32 (2022) 6811–6821.
- [10] Z. Chen, S. Geng, Y. Wang, Y. Wang, S. Song, Boosting 2 e[−] water oxidation reaction on WO₃ by F modification and revealing the mechanism by probing interfacial water structure, *Appl. Catal. B: Environ.* 317 (2022) 121756–121767.
- [11] L. He, Y. Ji, J. Cheng, C. Wang, L. Jiang, X. Chen, H. Li, S. Ke, J. Wang, Effect of pH and Cl[−] concentration on the electrochemical oxidation of pyridine in low-salinity reverse osmosis concentrate: kinetics, mechanism, and toxicity assessment, *Chem. Eng. J.* 449 (2022) 137669–137679.
- [12] S.P. Zheng, J.J. Jiang, A. van der Lee, M. Barboiu, A voltage-responsive synthetic Cl[−] channel regulated by pH, *Angew. Chem. Int. Ed.* 59 (2020) 18920–18926.
- [13] F. Wu, Y. Ping, Combining Landau–Zener theory and kinetic monte carlo sampling for small polaron mobility of doped BiVO₄ from first-principles, *J. Mater. Chem. A* 6 (2018) 20025–20036.
- [14] K. Zhou, W. Liu, P. Wang, J. Chen, H. Che, B. Liu, Y. Ao, Interfacial C–O covalent bonds improving the piezo-assisted photocatalytic performance of Bi₄Ti₃O₁₂@carbon schottky heterojunction, *Chem. Eng. J.* 480 (2024) 148012–478020.
- [15] X. Yan, G. Li, Z. Wang, Z. Yu, K. Wang, Y. Wu, Recent progress on piezoelectric materials for renewable energy conversion, *Nano Energy* 77 (2020) 105180–105238.
- [16] Q. Sun, D. Zhang, G. Xue, Q. Liu, X. Zhou, Z. Pei, H. Luo, L. Zhu, Piezo-assisted photoelectric catalysis degradation for dyes and antibiotics by Ag dots-modified NaNbO₃ powders, *Ceram. Int.* 48 (2022) 23182–23194.
- [17] H. Ding, N. Hadaeghi, M.-H. Zhang, T.-S. Jiang, A. Zintler, L. Carstensen, Y.-x. Zhang, H.-J. Kleebe, H.-b. Zhang, L. Molina-Luna, Translational antiphase boundaries in NaNbO₃ antiferroelectrics, *ACS Appl. Mater. Interfaces* 15 (2023) 59964–59972.
- [18] Q. Liu, F. Zhan, H. Luo, D. Zhai, Z. Xiao, Q. Sun, Q. Yi, Y. Yang, D. Zhang, Mechanism of interface engineering for ultrahigh piezo-photoelectric catalytic coupling effect of BaTiO₃@TiO₂ microflowers, *Appl. Catal. B: Environ.* 318 (2022) 121817.
- [19] Q. Liu, Z. Li, J. Li, F. Zhan, D. Zhai, Q. Sun, Z. Xiao, H. Luo, D. Zhang, Three dimensional BaTiO₃ piezoelectric ceramics coated with TiO₂ nanoarray for high performance of piezo-photoelectric catalysis, *Nano Energy* 98 (2022) 107267–107279.
- [20] S. Ji, H. Lei, M. Wu, Q. He, P. Sun, X. Dong, Piezoelectric polarization promoted spatial separation of photogenerated charges in Bi₂MoO₆ catalyst and investigation of its synergistic photopiezocatalytic activity, *J. Taiwan Inst. Chem. Eng.* 133 (2022) 104260–104269.
- [21] X. Xu, N. Yang, P. Wang, S. Wang, Y. Xiang, X. Zhang, X. Ding, H. Chen, Highly intensified molecular oxygen activation on Bi@Bi₂MoO₆ via a metallic Bi-coordinated facet-dependent effect, *ACS Appl. Mater. Interfaces* 12 (2019) 1867–1876.
- [22] Q. Fu, P. Liu, Y. Zhao, W. Liu, D. Zhan, J. Tian, B. Tan, C. Han, Composite heterojunction of BiFeO₃ and CdS: a photocathode for promoting efficient decomposition of water using piezoelectric photoelectrocatalysis, *J. Solid State Chem.* 331 (2024) 124515.
- [23] E. Khomyakova, M. Sadl, H. Ursic, J. Daniels, B. Malic, A. Bencan, D. Damjanovic, T. Rojac, Self-poling of BiFeO₃ thick films, *ACS Appl. Mater. Interfaces* 8 (2016) 19626–19634.
- [24] S. Singh, N. Khare, Coupling of piezoelectric, semiconducting and photoexcitation properties in NaNbO₃ nanostructures for controlling electrical transport: realizing an efficient piezo-photoanode and piezo-photocatalyst, *Nano Energy* 38 (2017) 335–341.
- [25] Y. Zhang, C. Cheng, Z. Zhou, R. Long, W.-H. Fang, Surface hydroxylation during water splitting promotes the photoactivity of BiVO₄(010) surface by suppressing polaron-mediated charge recombination, *J. Phys. Chem. Lett.* 14 (2023) 9096–9102.
- [26] H. Wu, L. Zhang, S. Qu, A. Du, J. Tang, Y.H. Ng, Polaron-mediated transport in BiVO₄ photoanodes for solar water oxidation, *ACS Energy Lett.* 8 (2023) 2177–2184.
- [27] J. Cen, S. Li, J. Zheng, F. Pan, Electron polarons in the subsurface layer of Mo/W-doped BiVO₄ surfaces, *RSC Adv.* 9 (2019) 819–823.
- [28] Q. Jing, Z. Liu, X. Cheng, C. Li, P. Ren, K. Guo, H. Yue, B. Xie, T. Li, Z. Wang, L. Shu, Boosting piezo-photocatalytic activity of BiVO₄/BiFeO₃ heterojunctions through built-in polarization field tailoring carrier transfer performances, *Chem. Eng. J.* 464 (2023) 464–475.
- [29] L. Liu, Z. Liu, M. Ruan, Z. Guo, C. Wang, Piezoelectric polarization assisted surface defect engineering to improve BiVO₄ photoelectrochemical water splitting, *Catal. Lett.* 36 (2024) 4630–4642.
- [30] H. Sun, W. Hua, S. Liang, Y. Li, J.-G. Wang, A self-adaptive semiconductor–liquid junction for highly active and stable solar water splitting, *J. Mater. Chem. A* 10 (2022) 20414–20423.
- [31] Z. Jiang, X. Zhu, Z. Wang, W. Liu, W. Yan, K. Sivula, J. Bao, Edge-sharing octahedrally coordinated Ni-Fe dual active sites on ZnFe₂O₄ for photoelectrochemical water oxidation, *Adv. Sci.* 10 (2023) 1869–1878.
- [32] S. Tang, W. Qiu, X. Xu, S. Xiao, Y. Tong, X. Wang, S. Yang, Harvesting of infrared part of sunlight to enhance polaron transport and solar water splitting, *Adv. Funct. Mater.* 32 (2022) 284–295.
- [33] H. Wang, Y.-I. Hu, G.-L. Song, D.-J. Zheng, Intrinsic and extrinsic doping to construct hematite nanorod p-n homojunctions for highly efficient PEC water splitting, *Chem. Eng. J.* 435 (2022) 135016–135028.
- [34] H. Choi, S. Seo, C.J. Yoon, J.B. Ahn, C.S. Kim, Y. Jung, Y. Kim, F.M. Toma, H. Kim, S. Lee, Organometal halide perovskite-based photoelectrochemical module systems for scalable unassisted solar water splitting, *Adv. Sci.* 10 (2023) 3106–3118.
- [35] J. Park, J. Kang, S. Chaule, J.-H. Jang, Recent progress and perspectives on heteroatom doping of hematite photoanodes for photoelectrochemical water splitting, *J. Mater. Chem. A* 11 (2023) 24551–24565.
- [36] M. Derbali, A. Othmani, S. Kouass, F. Touati, H. Dhaoui, BiVO₄/TiO₂ nanocomposite: electrochemical sensor for hydrogen peroxide, *Mater. Res. Bull.* 125 (2020) 110771–110805.
- [37] Z. Li, Q. Zhang, X. Chen, F. Yang, D. Wang, L. Liu, J. Ye, Cl[−] modification for effective promotion of photoelectrochemical water oxidation over BiVO₄, *Chem. Commun.* 56 (2020) 13153–13156.
- [38] J. Zhou, H. Cheng, J. Cheng, L. Wang, H. Xu, The emergence of high-performance conjugated polymer/inorganic semiconductor hybrid photoelectrodes for solar-driven photoelectrochemical water splitting, *Small Methods* 8 (2023) 418–436.
- [39] X. Zhang, H. Cui, M. Humayun, Y. Qu, N. Fan, X. Sun, L. Jing, Exceptional performance of photoelectrochemical water oxidation of single-crystal rutile TiO₂ nanorods dependent on the hole trapping of modified chloride, *Sci. Rep.* 6 (2016) 21430–21438.
- [40] H. Miao, Y. Sun, X. Zhou, Y. Li, F. Li, Piezoelectricity and ferroelectricity of cellular polypropylene electrets films characterized by piezoresponse force microscopy, *J. Appl. Phys.* 116 (2014) 4891395–4891404.
- [41] C. Zhang, Y. Shi, Y. Si, M. Liu, L. Guo, J. Zhao, O.V. Prezhdo, Improved carrier lifetime in BiVO₄ by spin protection, *Nano Lett.* 22 (2022) 6334–6341.
- [42] R.-T. Gao, X. Liu, X. Zhang, L. Wang, Steering electron transfer using interface engineering on front-illuminated robust BiVO₄ photoanodes, *Nano Energy* 89 (2021) 106360–106388.
- [43] J. You, C. Wang, Z. Guo, M. Ruan, Z. Liu, Lattice fluorine and adsorbed fluorine combine with piezoelectric polarization to boost the separation of bulk and surface carriers of Bi₂WO₆ for achieving efficient Piezo-PEC performance, *ACS Appl. Energy Mater.* 6 (2023) 8197–8208.
- [44] Z. Hao, M. Ruan, Z. Guo, W. Yan, X. Wu, Z. Liu, The synergistic role of the photosensitivity effect and extended space charge region in an inorganic–organic WO₃/PANI photoanode for efficient PEC water splitting, *Sustain. Energy Fuels* 5 (2021) 2893–2906.